

# Ballistic transport in AlAs two-dimensional electrons

O. Gunawan, Y. P. Shkolnikov, E. P. De Poortere, E. Tutuc, and M. Shayegan

*Department of Electrical Engineering, Princeton University, Princeton, New Jersey 08544*

(Dated: March 22, 2022)

We report the observation of commensurability oscillations in an AlAs two-dimensional electron system where two conduction-band valleys with elliptical in-plane Fermi contours are occupied. The Fourier power spectrum of the oscillations shows two frequency components consistent with those expected for the Fermi contours of the two valleys. From an analysis of the spectra we deduce  $m_l/m_t = 5.2 \pm 0.5$  for the ratio of the longitudinal and transverse electron effective masses.

Electrons confined to a modulation-doped AlAs quantum well are an emerging, high-mobility, two-dimensional electron system (2DES) with some unique properties that are very different from those of the more commonly studied GaAs 2DES [1, 2, 3]. The AlAs 2D electrons occupy multiple valleys in the conduction band, each with a large and anisotropic effective mass, and possess a much larger effective  $g$ -factor compared to GaAs 2D electrons. The combination of these properties has led to the observation of new phenomena in AlAs 2DES. Examples include magnetic phase transitions, marked by sharp resistance spikes, at Landau level crossings in tilted magnetic fields [3]. Also observed are fractional quantum Hall states at very high Landau level filling factors, stabilized possibly because of the multi-valley occupancy [1]. Here we report measurements of commensurability oscillations (COs) in a high-mobility AlAs 2DES subjected to a one-dimensional, lateral, periodic potential modulation. The 2D electrons in our system occupy two valleys with elliptical in-plane Fermi contours. The results demonstrate ballistic transport in a two-valley 2D system. Through Fourier and partial inverse Fourier analyses of the oscillations, we disentangle and study the COs of the electrons in the two valleys, and obtain their amplitude, phase and scattering time. More importantly, from an analysis of the CO frequencies, we determine the ratio of the longitudinal and transverse electron effective masses, a fundamental parameter that cannot be directly measured from other experiments on our 2DES.

In bulk AlAs, electrons occupy conduction band valleys centered at the six equivalent X points of the Brillouin zone. The Fermi surface consists of six, anisotropic, half-ellipsoids (three full-ellipsoids); we denote these ellipsoids (valleys) by X, Y, and Z, according to the direction of their major axes ( $x$ ,  $y$ , and  $z$ ). In a narrow (less than  $\sim 5$  nm wide) AlAs quantum well grown on a GaAs (001) substrate, thanks to its larger mass in the confinement direction, the Z valley (out-of-plane valley) has the lowest energy and is occupied by electrons [4]. For wider well widths, however, the strain from the lattice mismatch between GaAs and AlAs pushes the X and Y valleys (the in-plane valleys) down in energy with respect to the Z valley, so that now the X and Y valleys are occupied [5, 6, 7, 8, 9]. This is the case for the samples we have

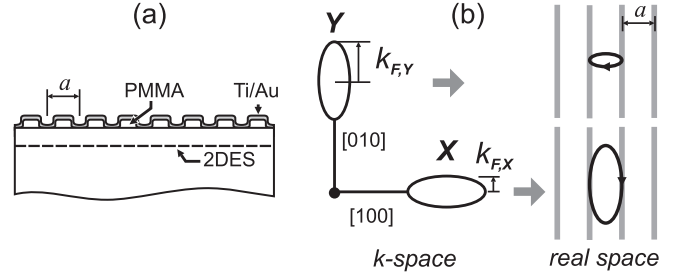


FIG. 1: (a) Schematic cross section of the device used to measure COs. Application of a bias to the Ti/Au surface gate with respect to the 2DES produces a potential modulation which is periodic in the  $[100]$  direction and has period  $a$ . (b) The AlAs in-plane valleys X and Y in  $k$ -space (left), and their corresponding first resonant CO orbits in real space (right) [14] are illustrated. The Fermi wave vectors  $k_{F,X}$  and  $k_{F,Y}$  relevant for the COs of the X and Y valley are also indicated.

studied.

Figure 1 highlights the basic principle of our study. Using a grating surface gate, we apply a lateral periodic potential with period  $a$  to the 2DES, and measure the low-field magneto-resistance ( $\rho_{xx}$ ) along the potential modulation direction as a function of a perpendicular magnetic field  $B$ . If transport is ballistic,  $\rho_{xx}$  oscillates with  $B$  as the classical electron cyclotron orbit diameter takes on values that are multiple integers of  $a$  [10, 11, 12, 13, 14]:

$$\rho_{xx} \propto \cos(2\pi f_{CO}/B - \pi/2) \quad (1)$$

$$f_{CO} = 2\hbar k_F / ea \quad (2)$$

where  $f_{CO}$  is the oscillation frequency and  $k_F$  is the Fermi wave vector perpendicular to the modulation direction (parallel to the grating stripes). Note that the oscillations are periodic in  $1/B$ . In our AlAs 2DES, there are two in-plane valleys occupied: X and Y. Their cyclotron orbits in real space have the same shape as their  $k$ -space orbits but rotated by  $90^\circ$  as shown in Fig. 1(b). If both valleys participate in the ballistic transport independently, we expect two superimposed sets of COs whose frequencies are related to the Fermi wave vectors parallel to the grating stripes as indicated in Fig. 1(b):

$$k_{F,X}^2 = 2\pi n_X \sqrt{m_t/m_l} \quad k_{F,Y}^2 = 2\pi n_Y \sqrt{m_l/m_t} \quad (3)$$

where  $n_X$  and  $n_Y$  are the 2D electron densities for the  $X$  and  $Y$  valleys respectively. These relations can be combined to yield:

$$\frac{m_l}{m_t} = \frac{f_{CO,Y}^2 n_X}{f_{CO,X}^2 n_Y} \quad (4)$$

implying that, if the valley densities are known, the frequencies of the COs can be used to directly determine the mass anisotropy ratio  $m_l/m_t$ , independent of  $a$ .

We used samples grown by molecular beam epitaxy on (001) GaAs substrates [1]. The 2DES is confined in an 11 nm-wide AlAs layer located at 110 nm below the surface and sandwiched between barrier layers of  $\text{Al}_{0.4}\text{Ga}_{0.6}\text{As}$ . It is modulation doped with a Si delta layer placed at a distance of 75 nm away. A Hall bar mesa was defined on each sample using standard photolithography and wet etching techniques. The Hall bar was aligned along the [100] direction so that the major axes of the two in-plane valleys were either parallel or perpendicular to the Hall bar. To fabricate the grating patterns, we spun 150 nm of polymethylmetacrylate (PMMA) on top of the sample, and used electron beam lithography to define an array of PMMA ridges with periods  $a$  equal to 300 and 400 nm. We then deposited 10 nm Ti and 30 nm Au to form a top gate. Biasing this top gate with respect to the 2DES results in a periodic potential modulation in the 2DES. Using illumination at low temperatures and front/back gate biasing, we varied the 2DES density between  $5$  to  $9 \times 10^{11} \text{ cm}^{-2}$ , with maximum mobility around  $9.3 \text{ m}^2/\text{Vs}$  prior to patterning the grating on top of the sample. We measured  $\rho_{xx}$  in a  $^3\text{He}$  cryostat with a base temperature of 0.35 K, and used a standard lock-in technique.

A typical  $\rho_{xx}$  vs.  $B$  trace, taken at  $T = 0.35 \text{ K}$  and total density  $n_{\text{tot}} = 8.7 \times 10^{11} \text{ cm}^{-2}$ , is shown in Fig. 2(a). It exhibits both COs, in the low field range  $-1 < B < 1 \text{ T}$ , and Shubnikov-de Haas oscillations (SdHOs), at  $B > 1.7 \text{ T}$ . The COs are more clearly seen in the second derivative ( $d^2\rho_{xx}/dB^2$ ) plot shown in the inset of Fig. 2(a). Fortunately, the COs and SdHOs are well separated in their field range, thus simplifying their analysis.

The SdHOs provide information regarding the electron densities of the 2DES and the valleys. In Fig. 2(c) we show the Fourier power spectrum of the SdHOs. To calculate this spectrum, we used the  $\rho_{xx}$  vs.  $1/B$  data for  $B > 1.7 \text{ T}$ , subtracted a second-order polynomial background, and multiplied the data by a Hamming window [15] in order to reduce the side-lobes in the spectrum. The spectrum exhibits three clear peaks, marked in Fig. 2(c) as  $n_{\text{tot}}$ ,  $n_{\text{tot}}/2$  and  $n_{\text{tot}}/4$ . The SdHO frequencies multiplied by  $e/h$  give the 2D density ( $e$  is the electron charge and  $h$  is the Planck's constant). We associate the  $n_{\text{tot}}$  peak with the total density, as the position of this peak multiplied by  $e/h$  indeed gives the total 2DES density which we independently determine from the Hall

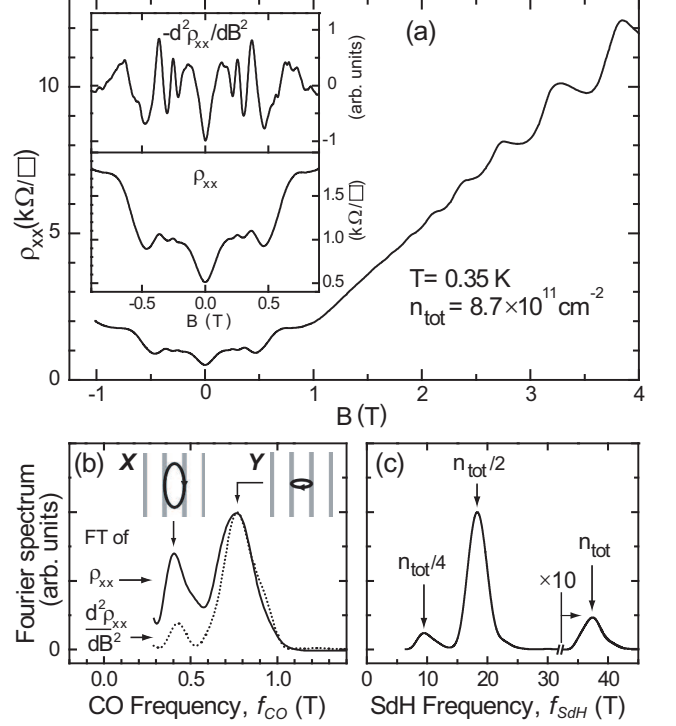


FIG. 2: (a) Magneto-resistance trace showing COs at low fields ( $-1 < B < 1 \text{ T}$ ) and SdHOs at high fields ( $B > 1.7 \text{ T}$ ) for a device with 400 nm grating period. Insets show the enlarged view of both  $\rho_{xx}$  and the numerically determined second derivative  $d^2\rho_{xx}/dB^2$ . (b) Fourier power spectra of COs from both  $\rho_{xx}$  (solid curve) and  $d^2\rho_{xx}/dB^2$  (dotted curve). The corresponding first resonant orbits in real space are shown above the peaks. (c) Fourier power spectrum of SdHOs.

coefficient. For the data shown in Fig. 2, we deduce  $n_{\text{tot}} = n_X + n_Y = 8.7 \times 10^{11} \text{ cm}^{-2}$ . The presence of the  $n_{\text{tot}}/4$  peak indicates the spin and valley degeneracy of the system [16].

Figure 2 (b) shows the Fourier power spectra of COs calculated using  $\rho_{xx}$  and  $d^2\rho_{xx}/dB^2$  vs.  $1/B$  data in the  $0.1 < B < 1 \text{ T}$  range. Both spectra exhibit two clear peaks at  $f_{\text{CO},X}$  and  $f_{\text{CO},Y}$ , which we associate with the CO frequencies of the  $X$  and  $Y$  valleys, respectively. If we assume that the two valleys have equal densities, we can use Eq. (4) to immediately find  $m_l/m_t \simeq 4.4$ . This value, however, is inaccurate because there is a small but finite imbalance between the  $X$  and  $Y$  valley densities in our sample. Such imbalances can occur because of anisotropic strain in the plane of the sample and are often present in AlAs 2DESs. Note that the Fourier spectrum of the SdHOs cannot resolve small valley density imbalances. As detailed in the next paragraph, we analyze the dependence of CO frequencies on density to deduce the imbalance between the valley densities, and also to determine the  $m_l/m_t$  ratio more accurately.

Figure 3 summarizes the density dependence of our CO

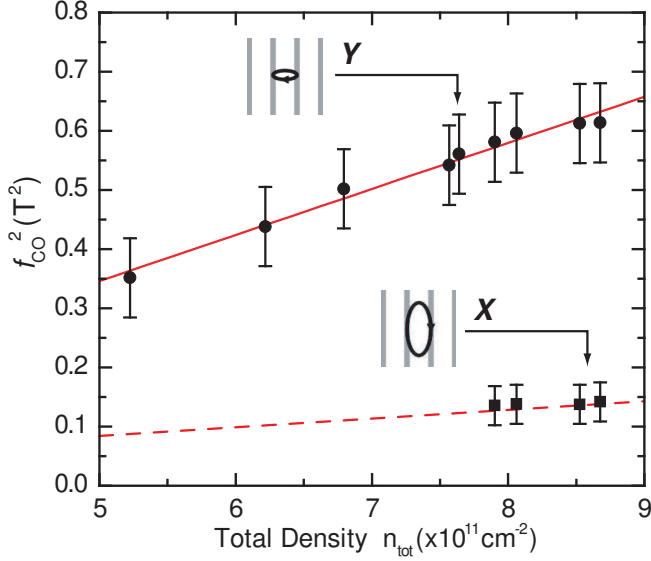


FIG. 3: Density dependence of the CO frequencies for the Y (circles) and X valleys (squares). The line through the circles is a least-squares fit to the data; its slope determines the ratio  $m_l/m_t$  and its intercept the density difference  $\Delta n$  of the two valleys. The dashed line is described in the text.

frequencies. Denoting the difference between the valley densities by  $\Delta n = n_Y - n_X$ , we can rewrite Eqs. (2) and (3) as:

$$f_{CO,Y}^2 = \frac{h^2}{\pi e^2 a^2} \sqrt{\frac{m_l}{m_t}} (n_{tot} + \Delta n) \quad (5)$$

$$f_{CO,X}^2 = \frac{h^2}{\pi e^2 a^2} \sqrt{\frac{m_t}{m_l}} (n_{tot} - \Delta n). \quad (6)$$

From the slope and intercept of the  $f_{CO}^2$  vs.  $n_{tot}$  plots, we can deduce the  $m_l/m_t$  ratio and  $\Delta n$ . Concentrating on the Y valley, a least-squares fit of  $f_{CO,Y}^2$  data points (circles in Fig. 3) to a line leads to values  $m_l/m_t = 5.2 \pm 0.5$  and  $\Delta n = (-0.6 \pm 0.4) \times 10^{11} \text{ cm}^{-2}$ . Note that such a small value of  $\Delta n$  is consistent with the nearly valley-degenerate picture deduced from the existence of the  $n_{tot}/4$  peak in the SdH frequency spectrum [Fig. 2(c)].

The above determination of the  $m_l/m_t$  ratio is based on the density dependence of  $f_{CO,Y}$  only and does not use the measured  $f_{CO,X}$ . As a consistency check, we can use Eq. (6) to predict  $f_{CO}$  for the X valley using  $m_l/m_t$  and  $\Delta n$  deduced from the above analysis of  $f_{CO,Y}$ . This prediction, shown as a dashed line in Fig. 3, is in good agreement with the measured  $f_{CO,X}$  (solid squares). This consistency confirms that we are indeed observing COs for both valleys.

We have repeated similar experiments in a sample from a different wafer, containing a 2DES confined to a 15 nm wide AlAs quantum well. In this sample only the COs of the Y valley could be reliably determined. By performing

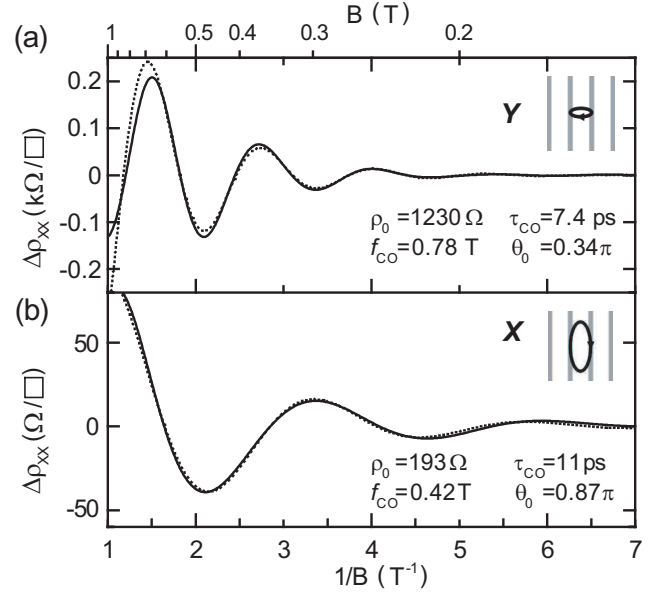


FIG. 4: Results of the inverse Fourier decomposition of the COs of Fig. 2 for the Y and X valleys. The dotted curves show the best fits of Eq. (7) using the indicated parameters.

similar analysis using Eq. (5), in the density range from  $5.5$  to  $9 \times 10^{11} \text{ cm}^{-2}$ , we deduce  $m_l/m_t \simeq 5.4$ , in good agreement with the results presented here.

At this point it is worthwhile emphasizing that the COs described here uniquely probe the  $m_l/m_t$  ratio [17]. Conventional experiments that probe the effective mass, such as cyclotron resonance or measurements of the temperature dependence of the amplitude of the SdHOs, lead to a determination of the cyclotron effective mass,  $m_{CR}$ . In a 2DES with an elliptical Fermi contour,  $m_{CR}$  is equal to  $(m_l m_t)^{1/2}$ , and therefore provides information complementary to the  $m_l/m_t$  ratio, so that  $m_l$  and  $m_t$  can be determined. In fact, using the measured  $m_{CR} = 0.46 m_e$  in AlAs 2DESs [18], we can use the  $m_l/m_t = 5.2 \pm 0.5$  ratio to deduce  $m_l = (1.1 \pm 0.1) m_e$  and  $m_t = (0.20 \pm 0.02) m_e$ . These values are in good agreement with the (theoretical) value of  $m_t = 0.19 m_e$  that is calculated in Ref. [17], and  $m_l = 1.1 m_e$  that is deduced from the Faraday rotation measurements [17]; they also agree well with the results of the majority of theoretical and experimental determinations of the effective mass in AlAs.

We proceed to extract more information, such as the amplitude, phase, and scattering time for the COs of each valley by performing partial inverse Fourier analysis. Figure 4 summarizes the results of such analysis. The Fourier power spectrum shown in Fig. 2(b) is separated into two regions chosen to isolate the two CO peaks. The region corresponding to COs of Y valley ( $0.57 < f_{CO} < 1.21 \text{ T}$ ) is inverse Fourier transformed and divided by the original window function. The result is shown as the solid curve in Fig. 4(a). The region corresponding to the COs

of  $X$  valley ( $0.29 < f_{CO} < 0.57$  T), is analyzed in the same manner and the result is shown by the solid curve in Fig. 4(b) [19].

We fit the deduced COs for each valley to a simple expression that assumes the amplitude of the COs decreases exponentially with  $1/B$ :

$$\Delta\rho_{xx} \propto \rho_0 \exp(-\pi/\omega_c \tau_{CO}) \cos(2\pi f_{CO}/B - \theta_0) \quad (7)$$

where  $\rho_0, \tau_{CO}, f_{CO}$ , and  $\theta_0$  are the fitting parameters;  $\omega_c = eB/m_{CR}$  is cyclotron frequency with  $m_{CR} = (m_l m_t)^{1/2} = 0.46m_e$ . The exponential term of expression (7) is analogous to the Dingle factor used to describe the damping of the SdHOs' amplitude with increasing  $1/B$ , and has been used successfully to fit COs in GaAs 2D electrons [20] and holes [21]. In Fig. 4 the results of the best fits are shown as dotted curves along with their fitting parameters. The best-fit  $\theta_0$  for the COs of  $Y$  and  $X$  valleys are  $0.34\pi$  and  $0.87\pi$  respectively, in reasonable agreement with the expected value of  $0.5\pi$  (the relative phase errors are 8% and 18% of  $2\pi$ ). This consistency affirms that the reconstructed oscillations faithfully represent the COs of the two in-plane valleys. The amplitude of the oscillations for the  $Y$  valley is significantly larger than for the  $X$  valley as expected from the shorter real-space, resonant orbital trajectories for this valley [Fig. 1(b)]. On the other hand, the scattering times,  $\tau_{CO}$ , that we deduce from the fits are comparable for the two valleys, suggesting that scattering is nearly isotropic.

We also deduce two other scattering times: the quantum lifetime  $\tau_{SdH}$  and the mobility scattering time  $\tau_\mu$ , and compare them with  $\tau_{CO}$ . From fitting the  $B$  dependence of the amplitude of the SdHOs to the damping factor  $\exp(-\pi/\omega_c \tau)$ , we obtain  $\tau_{SdH} = 0.76$  ps. The mobility scattering time is  $\tau_\mu = 24$  ps, determined from the mobility of the same sample prior to patterning. Similar to CO experiments in other 2D carrier systems [20, 21], we observe  $\tau_{SdH} < \tau_{CO} < \tau_\mu$ . This observation can be qualitatively understood considering the sensitivity of these  $\tau$  to the scattering angle [20]:  $\tau_\mu$  is the longest since the mobility is least sensitive to small-angle scattering, while  $\tau_{SdH}$  is the shortest because the SdHOs are sensitive to all scattering events.

We close by reflecting on possible future studies where ballistic transport in AlAs 2DESs can be applied. One possibility is to apply the periodic potential along different in-plane directions and map out the Fermi contour shape [22]. A second area involves studies of ballistic *spin polarized* currents. Because of the large values of effective mass and  $g$ -factor [23] of AlAs 2D electrons, it is sufficient to apply an in-plane magnetic field of only a few T to fully spin-polarize the electrons. Such studies are of substantial current interest as they have relevance for spintronic devices. A third area concerns chaotic transport in anti-dots; the highly anisotropic electron Fermi contours of AlAs 2D electrons should lead to interesting

phenomena, examples of which have been reported recently in GaAs 2D hole systems which also possess non-circular Fermi contours [24].

We thank the NSF and ARO for supporting this work, and J. J. Heremans and R. Winkler for illuminating discussions.

- 
- [1] E. P. De Poortere *et al.*, Appl. Phys. Lett. **80**, 1583 (2002).
  - [2] Y. P. Shkolnikov *et al.*, Phys. Rev. Lett. **89**, 226 805 (2002).
  - [3] E. P. De Poortere *et al.*, Phys. Rev. Lett. **91**, 216 802 (2003).
  - [4] This is similar to (001) Si-MOSFETs, except that in the Si case the 2D electrons occupy *two* out-of-plane valleys at equivalent points along the Brillouin zone  $\Delta$  lines.
  - [5] T. P. Smith, III, *et al.*, Phys. Rev. B **35**, 9349 (1987); Surf. Sci. **196**, 287 (1988).
  - [6] H. W. van Kesteren *et al.*, Phys. Rev. B **39**, 13 426 (1989).
  - [7] K. Maezawa, T. Mizutani, and S. Yamada, J. Appl. Phys. **71**, 296 (1992).
  - [8] T. S. Lay *et al.*, Appl. Phys. Lett. **62**, 3120 (1993).
  - [9] S. Yamada, K. Maezawa, W. T. Yuen, and R. A. Stradling, Physica B **201**, 295 (1994).
  - [10] D. Weiss *et al.*, Europhys. Lett. **9**, 179 (1989).
  - [11] R. R. Gerhardts *et al.*, Phys. Rev. Lett. **62**, 1173 (1989).
  - [12] R. W. Winkler *et al.*, Phys. Rev. Lett. **62**, 1177 (1989).
  - [13] C. W. J. Beenakker, Phys. Rev. Lett. **62**, 2020 (1989).
  - [14] More precisely, as Eq. (1) indicates, a maximum in  $\rho_{xx}$  is seen whenever the cyclotron orbit diameter equals  $a(p + 1/4)$ , where  $p$  is an integer. In Fig. 1(b), for simplicity, we schematically show the condition for the first resonance as when the diameter is equal to  $a$ .
  - [15] S. K. Mitra and J. F. Kaiser, *Handbook for Digital Signal Processing* (Wiley, New York, 1993), p. 1157.
  - [16] As detailed in Ref. [2], the spin and valley degeneracies are lifted at higher  $B$ , leading to the presence of the  $n_{tot}/2$  and  $n_{tot}$  peaks in the Fourier spectrum.
  - [17] Faraday rotation experiments can also determine the  $m_l/m_t$  ratio, but such determination requires knowing  $m_l$  or  $m_t$  and the  $\langle\tau^2\rangle/\langle\tau\rangle^2$  ratio where  $\tau$  is the scattering time. In fact, B. Rheinländer *et al.* [Phys. Stat. Sol. B **49**, K167 (1972)] used Faraday rotation measurements in bulk AlAs and, assuming  $m_t = 0.19m_e$  (determined from a  $\mathbf{k}\cdot\mathbf{p}$  calculation) and  $\langle\tau^2\rangle/\langle\tau\rangle^2 = 1$ , deduced a ratio  $m_l/m_t = 5.7$ .
  - [18] The most accurate cyclotron resonance (CR) measurements in AlAs 2DESs so far were reported by T.S. Lay *et al.* [8], and yielded  $m_{CR} = (0.46 \pm 0.02)m_e$ . This value is in very good agreement with the results of CR measurements by N. Miura *et al.* [Solid State Commun. **79**, 1039 (1991)] on  $n$ -type AlAs layers ( $m_{CR} = (0.47 \pm 0.01)m_e$ ), and by T. P. Smith, III, *et al.* [5] on 2DESs in multiple AlAs quantum wells ( $m_{CR} \simeq 0.5m_e$ ); the latter data, however, show a very broad CR. There was also a CR study of GaAs/AlAs short-period superlattices by H. Momose *et al.* [Physica E **4**, 10 (1999)], where  $m_t = 0.21m_e$  and  $m_l = 1.04m_e$  were deduced. A summary and discussion of AlAs effective masses can be found in [Q. Guo *et*

- al.*, Phys. Stat. Sol. B **197**, 111 (1996)].
- [19] If we subtract the sum of the CO traces deduced for the individual valleys (shown in Fig. 4) from the original CO trace of Fig. 2(a), we obtain a featureless, non-oscillatory background signal.
- [20] J. P. Lu and M. Shayegan, Phys. Rev. B **58**, 1138 (1998).
- [21] J. P. Lu *et al.*, Phys. Rev. B **60**, 13 776 (1999).
- [22] See, e.g., J. J. Heremans *et al.*, Surf. Sci. **305**, 348 (1994).
- [23] S. J. Papadakis *et al.*, Phys. Rev. B **59**, 12 743 (1999).
- [24] M. Zitzlsperger *et al.*, Europhys. Lett. **61**, 382 (2003).